Optical Properties of Zn†

L. P. MOSTELLER, JR.,* AND F. WOOTEN
Lawrence Radiation Laboratory and Department of Applied Science, University of California, Livermore, California

(Received 25 January 1968)

The basal-plane reflectance of single crystals of high-purity (99.999%) Zn, cleaved and maintained in a vacuum chamber at pressures less than 10^{-9} Torr, has been measured in the wavelength region $1150 \leq \lambda \leq 5600$ Å. All measurements were made at 96°K. The shape of the reflectance curve for the ultraviolet region is quite accurately calculated on the basis of a free-electron model using the relaxation time, $\tau_c = 3.2 \times 10^{-14}$ sec, calculated from the dc electrical conductivity at 96°K, and an optical mass $m_a = 2.04$. The magnitude of the reflectance, about 85% just below the plasma frequency, is less than that calculated for the free-electron model. The difference is presumably the effect of interband transitions. The plasma resonance occurs at 10.1 eV. The experiments clearly demonstrate the necessity of an atomically clean surface for meaningful reflectance measurements in the vacuum ultraviolet.

INTRODUCTION

THE work reported here is the first on the vacuum ultraviolet optical properties of single-crystal Zn. Earlier work has been mostly confined to evaporated films or crystals studied in the visible and near-infrared regions.[1–8]

We have measured the basal-plane reflectance of single crystals of high-purity (99.999%) Zn. The crystals were cleaved and maintained in a vacuum chamber at pressures less than 10^{-9} Torr, except for one study of the effects of contamination. All measurements were made at temperatures of about 96°K, a temperature at which Zn cleaves easily. The reflectance was measured for the wavelength region $1150 \leq \lambda \leq 5480$ Å.

We first describe the experimental apparatus and techniques used to obtain the optical properties. Next we use the data presented here, as well as some of that from earlier studies, in an examination of the optical properties of Zn in terms of a free-electron model. We then consider plasma effects, interband transitions, and sum rules.

APPARATUS

A schematic sketch of the apparatus is shown in Fig. 1. A McPherson model 225 vacuum monochromator with a hydrogen-discharge Hinteregger-type light source was used for $1150 < \lambda \leq 2800$ Å. A mercury-discharge lamp was used for $2800 \leq \lambda < 5480$ Å, and a calcite polarizer was also used sometimes in this spectral region.

A stainless-steel bellows on the sample chamber is centered 60° off the normal to the reflecting surface of the specimen, and is continuously rotatable from 50° to 70°. Another radiation entry port is fixed at 25° and, when used, a 5-in. spacer tube is placed between it and the lens system to compensate for the length of the bellows. This allows the same lens system to be used with either radiation port. Each port has a LiF window so that ultraviolet light can be transmitted into the chamber while pressures less than 10^{-9} Torr are maintained within the chamber.

The crystal cleaver assembly is much like that described by Kindig and Spicer.[9] It serves two purposes: It is used for cleaving the crystal, and for moving the crystal into the crystal holder.

A crystal holder is mounted on the bottom of a Dewar (not shown in Fig. 1) which protrudes down into the sample chamber.

The detector assembly within the sample chamber consists of a photodiode, a rotation mechanism, and a Varian magnetic rotary feedthrough. The assembly is mounted to a flange on the bottom of the chamber. A photodiode position indicator consisting of a fixed vernier and a rotatable circular scale is connected to the bottom of the rotary feedthrough. The position of the photodiode can be read to ±0.02°. The photodiode can be swung in an arc about the shaft of the rotary feedthrough; it can also be rotated 180° with respect to the support arm connecting it to the feedthrough shaft.

The light chopper has four equally spaced blades at 45° to the axis of rotation. This produces two alternating light beams, one perpendicular to and the other collinear with the original beam. The perpendicular beam illuminates a photodiode which produces a reference signal proportional to the intensity of the beam. The collinear beam passes through the focusing lens and the LiF window and into the high-vacuum

† Work performed under the auspices of the U. S. Atomic Energy Commission.

* Major, U. S. Air Force. Present address: Hq. DASA, Washington, D. C. 20301.

[1] A. P. Lenham and D. M. Treherne, Proc. Phys. Soc. (London) 83, 1059 (1964).
[2] A. P. Lenham and D. M. Treherne, J. Opt. Soc. Am. 56, 752 (1966).
[3] A. P. Lenham, D. M. Treherne, and A. J. Woodall, in *Optical Properties and Electronic Structure of Metals and Alloys*, edited by F. Abeles (North-Holland Publishing Co., Amsterdam, 1966).
[4] A. H. Lettington, in *Optical Properties and Electronic Structure of Metals and Alloys*, edited by F. Abeles (North-Holland Publishing Co., Amsterdam, 1966).
[5] T. M. Jelinek, R. N. Hamm, and E. T. Arakawa, Oak Ridge National Laboratory Report No. TM-1164, August, 1965 (unpublished).
[6] G. Pfestorf, Ann. Physik 81, 906 (1926).
[7] G. B. Sabine, Phys. Rev. 55, 1064 (1939).
[8] W. Meier, Ann. Physik 31, 1017 (1910).
[9] N. B. Kindig and W. E. Spicer, Phys. Rev. 138, A561 (1965).

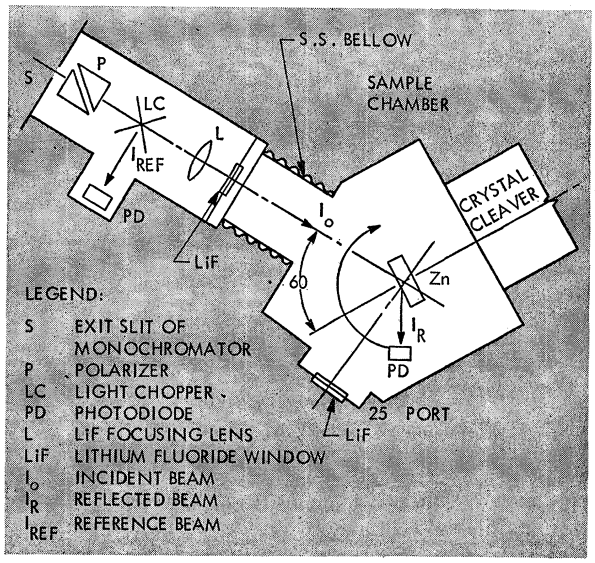

FIG. 1. Schematic drawing of vacuum reflectometer.

chamber where it illuminates the rotary photodiode either as the incident beam or as the reflected beam from the specimen.

Electrical currents from the photodiodes were measured with the aid of picoammeters and lock-in amplifiers, displayed on digital voltmeters, and then recorded by hand.

REFLECTANCE MEASUREMENT TECHNIQUES

Measurement of the reflectance is a two-step process. First, the ratio $R_1(\lambda)=I_o/I_{\text{ref}}$ is determined over a range of wavelengths. Here, I_o is the intensity of the beam incident on the specimen and I_{ref} is the intensity of the reference beam reflected by the light chopper. Second, the photodiode within the sample chamber is positioned to detect the radiation reflected from the specimen and the ratio $R_2(\lambda)=I_R/I_{\text{ref}}$ is determined. The reflectance of the sample is then $R(\lambda)=R_2(\lambda)/R_1(\lambda)$.

The angle of incidence is determined by measuring the angular position of the incident and reflected beams with the photodiode inside the sample chamber. The photodiode is constructed with a square mask as illustrated in Fig. 2. The photodiode is positioned to detect either the incident or reflected beam, and is then rotated from left to right until the right edge of the mask just clears the left edge of the light beam, as illustrated by the solid lines in Fig. 2. This angular position of the photodiode is recorded. Next, the photodiode is rotated from left to right until the left edge of the mask just clears the right edge of the beam (broken lines in Fig. 2). The mean of these two angular positions of the photodiode is the angular position of the light beam. The angle of incidence is half the difference between the angular positions of the incident and reflected beams.

Errors due to misalignment of the crystal face with respect to the rotary feedthrough shaft, angle-of-incidence measurements, and other sources are usually negligible, or appropriate corrections can be made. Considering all sources of error, it is estimated that the measured reflectance is accurate to within 5%.

REFLECTANCE DATA

Zinc crystals are uniaxial, thus the interaction of light with Zn is determined by the complex dielectric functions ϵ_{11} and ϵ_{1}, according to whether the electric vector is parallel or perpendicular to the optic axis. At an arbitrary angle of incidence, the interaction is a function of the angle and both dielectric functions. The optical constants can be determined from the reflectance at normal incidence by means of a Kramers-Kronig analysis,[10] but such an analysis typically requires extrapolation of reflectance data to wavelengths outside the range of measurements. The extrapolation is often of dubious validity and, especially if the region of extrapolation is one of appreciable reflectivity, is likely to be fraught with errors.[11,12] Because the reflectance of Zn is very high over nearly the entire wavelength region of measurements reported here, a Kramers-Kronig analysis is not suitable. If a Kramers-Kronig analysis is not to be used, the determination of the real (n_{11},n_1) and imaginary (k_{11},k_1) parts of the complex indices of refraction $\hat{n}_{11}$ and $\hat{n}_1$ requires four independent measurements for each wavelength.

It is usually desirable to work with polarized light, and we have made some measurements using polarized light, but it is not convenient in the vacuum ultraviolet. We have thus chosen to measure the reflectance at four different angles of incidence. Measurements of

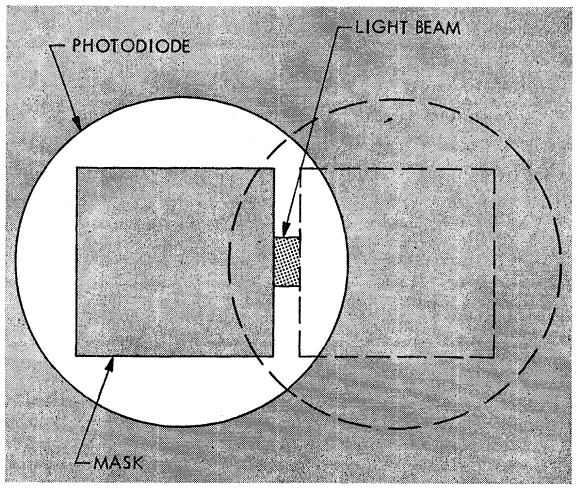

FIG. 2. Illustration of angle-of-incidence measurement.

[10] H. R. Philipp and E. A. Taft, Phys. Rev. 113, 1002 (1959).
[11] D. Beaglehole, Proc. Phys. Soc. (London) 85, 1007 (1965).
[12] F. Stern, in *Solid State Physics*, edited by F. Seitz and D. Turnbull (Academic Press Inc., New York, 1963), Vol. 15.

reflectance at different angles have been found to give results equal to or better than those obtained from a Kramers–Kronig analysis[11,13]; the only disadvantages are the minor one that a larger number of reflectance measurements must be made, and, somewhat more than minor, the fact that the angle of incidence must be determined with great care.

Consider a light ray incident onto the basal plane of Zn at an angle θ_i with respect to the surface normal, i.e., to the optic axis. The incident light ray and the optic axis define the plane of incidence. The reflectance for light polarized such that the electric vector is perpendicular to the plane of incidence, and hence perpendicular to the optic axis, is

$$R_\perp=\frac{(\cos\theta_i-a_\perp)^2+b_\perp^2}{(\cos\theta_i+a_\perp)^2+b_\perp^2}, \tag{1}$$

where

$$2\begin{Bmatrix}a_\perp^2\\ b_\perp^2\end{Bmatrix}=[(n_\perp^2-k_\perp^2-\sin^2\theta_i)^2+4n_\perp^2k_\perp^2]^{1/2} \pm(n_\perp^2-k_\perp^2-\sin^2\theta_i).$$

The reflectance for light polarized such that the electric vector is parallel to the plane of incidence is

$$R_{\parallel}=\frac{(c\cos\theta_i-a_{\parallel})^2+(d\cos\theta_i-b_{\parallel})^2}{(c\cos\theta_i+a_{\parallel})^2+(d\cos\theta_i+b_{\parallel})^2}, \tag{2}$$

where

$$c=n_{\parallel}n_\perp-k_{\parallel}k_\perp,$$
$$d=n_\perp k_{\parallel}+n_{\parallel}k_\perp,$$
$$2\begin{Bmatrix}a_{\parallel}^2\\ b_{\parallel}^2\end{Bmatrix}=[(n_{\parallel}^2-k_{\parallel}^2-\sin^2\theta_i)^2+4n_{\parallel}^2k_{\parallel}^2]^{1/2} \pm(n_{\parallel}^2-k_{\parallel}^2-\sin^2\theta_i).$$

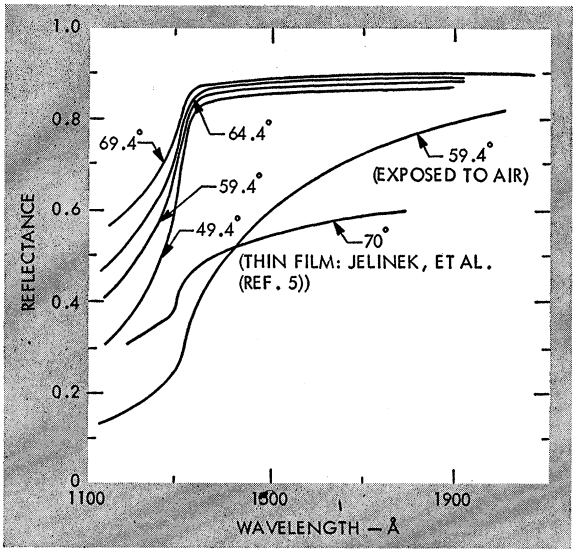

FIG. 3. Reflectance of Zn for nonpolarized light.

[13] D. C. Hinson and J. R. Stevenson, Phys. Rev. **159**, 711 (1967).

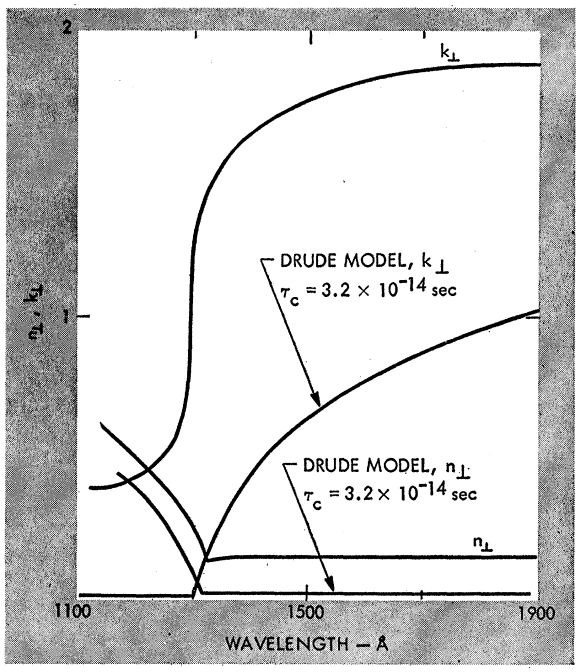

FIG. 4. Optical constants for basal plane of Zn.

The reflectance for nonpolarized light is given by

$$R(n_\perp,k_\perp,n_{\parallel},k_{\parallel},\theta_i)=\tfrac{1}{2}[R_{\parallel}+R_\perp]. \tag{3}$$

Equation (3) requires a trivial modification for partially polarized light.

In this work we have solved Eq. (3) with a digital computer. We have previously checked the computer program with a number of test cases, using exact reflectance data computed from Eqs. (1)–(3). In each case the correct solution was obtained. Details of the computer program, as well as a derivation of Eqs. (1) and (2), have been published.[14]

The measured reflectance for nonpolarized radiation and the computed optical constants for the electric vector perpendicular to the optic axis are presented in Figs. 3–6 for the most interesting region in the vacuum ultraviolet. The optical constants for the electric vector parallel to the optic axis are not presented because the reflectance for the basal plane of Zn is relatively insensitive to $n_{\parallel}$ and $k_{\parallel}$ for the angles of incidence used here. This can be understood by decomposing the radiation into two beams, one polarized normal to the plane of incidence and the other parallel to it. For the angles of incidence used in this work, the reflectance for the normal beam and about half the contribution to the reflectance for the parallel beam are determined by $n_\perp$, $k_\perp$. Thus the reflectance for nonpolarized radiation is about three times more sensitive to $n_\perp$, $k_\perp$ than to $n_{\parallel}$, $k_{\parallel}$. In addition, in the solution for the optical constants, $n_\perp$ usually converges faster than $k_\perp$ which converges

[14] L. P. Mosteller, Jr., and F. Wooten, J. Opt. Soc. Am. **58**, 511 (1968).

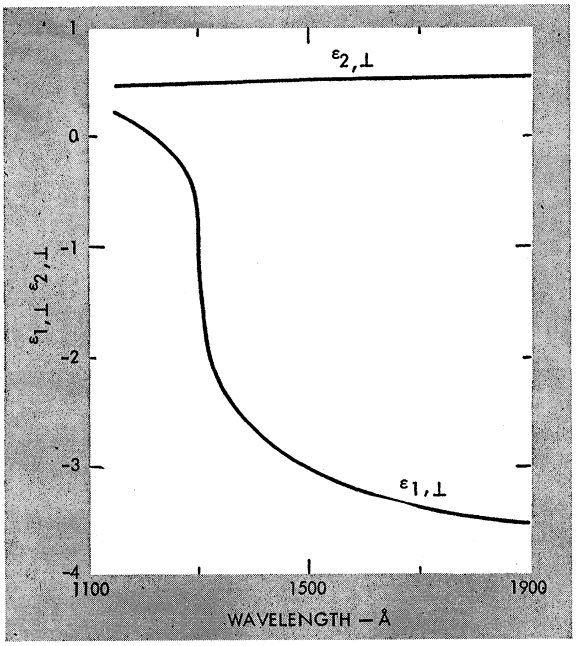

FIG. 5. Dielectric functions for basal plane of Zn.

much faster than either $n_{\parallel}$ or $k_{\parallel}$. It is also likely that there is little difference between $n_{\perp}$ and $n_{\parallel}$ or between $k_{\perp}$ and $k_{\parallel}$ in the vacuum ultraviolet, for Zn is a very free-electron-like metal.

The measured reflectance R for four different angles of incidence is presented in Fig. 3 for $1150 \leq \lambda \leq 1900$ Å. For $1900 \leq \lambda \leq 5600$ Å, R is nearly constant. Although $R_{\perp}$ and $R_{\parallel}$ were measured $\lambda \geq 2800$ Å, they are not presented because they also are constant within experimental error. During these measurements, the temperature of the crystal was maintained at 96°K and the slits of the monochromator were set at 0.8 mm thus corresponding to a band pass of 13 Å. The pressure in the chamber was less than 10^{-9} Torr.

After the reflectance had been measured for the freshly cleaved crystal, the liquid nitrogen removed from the Dewar, and the crystal returned to room temperature, the reflecting surface was contaminated by introducing air into the system. Then, after exposing the crystal to atmospheric pressure for 7 min, the chamber was evacuated to a pressure of about 10^{-8} Torr, the crystal was again cooled to 96°K, and the reflectance for an angle of incidence of 59.4 was measured for $1150 \leq \lambda \leq 2000$ Å. The results are shown in Fig. 3; they clearly demonstrate the importance of a truly clean reflecting surface in the vacuum ultraviolet. Also shown in Fig. 3 is the reflectance of a vacuum evaporated film of Zn as measured by Jelinek *et al.*[5] They evaporated the Zn in a bell jar at pressures of about 10^{-6} Torr and then transferred the sample to the reflectivity chamber within several minutes after evaporation. The average film thickness for their samples was about 800 Å.

FREE-ELECTRON MODEL

Zinc has optical properties similar to aluminum. There are prominent interband transitions in the infrared and visible ranges, but the reflectance remains high well into the vacuum ultraviolet, where at 1310 Å it drops quickly. This suggests that Zn can be characterized by a modified Drude model in which the reflectance is lower than that predicted by the classical Drude model alone because of the effects of interband transitions.

We now examine Zn on the basis of a nearly-free-electron model. Following Ehrenreich *et al.*,[15] we express the dielectric functions of the electron gas as

$$\epsilon_1^{(f)} = n^2 - k^2 = 1 - \omega_{p_a}^2/(\omega^2 + \tau_c^{-2}), \quad (4)$$

$$\epsilon_2^{(f)} = 2nk = \omega_{p_a}^2/\omega\tau_c(\omega^2 + \tau_c^{-2}). \quad (5)$$

Here the plasma frequency is

$$\omega_{p_a} = (4\pi N e^2/m_a)^{1/2}, \quad (6)$$

τ_c is the relaxation time, N is the conduction-electron density, and m_a is the optical mass. We shall find it useful to also write the plasma frequency in terms of the atomic density N_a and an effective number of electrons per atom, n_{eff}. Thus,

$$\omega_{p_a}^2 = (4\pi N_a e^2/m) n_{\text{eff}}, \quad (7)$$

where m is the free-electron mass.

The reflectance for normal incidence,

$$R - \frac{(n-1)^2 + k^2}{(n+1)^2 + k^2}, \quad (8)$$

is evaluated in the Drude model by replacing n and k by the solutions of Eqs. (4) and (5). To evaluate Eq. (8) in the Drude model requires knowing ω_{p_a} and τ_c.

We have chosen the plasma frequency ω_{p_a} as 1.44×10^{16} sec^{-1}, corresponding to the sharp knees in the reflectance curves of Fig. 2 at $\lambda_{p_a} = 1310$ Å. The

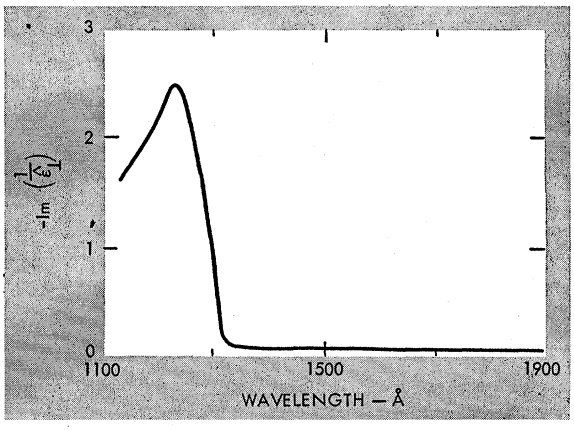

FIG. 6. Energy-loss function for basal plane of Zn.

[15] H. Ehrenreich, H. R. Philipp, and B. Segall, Phys. Rev. **132**, 1918 (1963).

knees in these curves are characteristic of a free-electron gas at the onset of the region of plasma excitation.[16] In the present case they are remarkably close to the ideal shape for a free-electron gas; the knees are even more sharply defined than for Al. The wavelength 1310 Å corresponds to $n_{\text{eff}}=0.98$ and to an optical mass $m_a=2.04$.

The lifetime is determined from the dc electrical conductivity,

$$\sigma_o=ne^2\tau_c/m. \tag{9}$$

Using the experimental value of σ_o at 96°K, i.e., 5.9×10^5 Ω^{-1}-cm^{-1}, and the free-electron mass, τ_c is found to be 1.6×10^{-14} sec. If the effective mass determined from Eq. (6) is used in Eq. (9), τ_c is found to be 3.2×10^{-14} sec.

We emphasize that we are fitting data for the uv reflectance of Zn to a nearly free-electron model. Our approach thus differs from that of Ehrenreich *et al.*[15] They were able to determine the intraband optical properties of Al from reflectance data for wavelengths sufficiently long that interband effects could be neglected. Such data are not available for Zn. There is, however, a significant difference in the uv reflectance of Zn compared with that reported for other materials; the reflectance curve for Zn is so strikingly similar to that for a free-electron gas that it leaves no choice but to attempt a quantitative comparison with a free-electron model.

Figure 7 shows a comparison of the reflectance for normal incidence calculated from Eq. (8), using the free-electron model, with the computed from the experimental values for n_1 and k_1. Curve I is drawn with $\tau_c=3.2\times10^{-14}$ sec. Curve III was computed from the experimental optical constants. The close agreement in shape of curves I and III, and especially the position and curvature of the knees, supports our choice of ω_{p_a} and τ_c and lends support to the general validity of the free-electron model as well. The lack of agreement is only in the absolute magnitudes of the reflectances. Curve II is drawn with $\tau_c=2.3\times10^{-15}$ sec. The magnitude of the reflectance for curve II is in good agreement with that for curve III, but the shape of the knee is wrong.

The curves presented in Fig. 7 indicate that the shape of the reflectance curve for Zn is quite accurately calculated on the basis of a free-electron model using the relaxation time determined from the dc electrical conductivity. The difference in magnitude between curves I and III may arise simply because the measured reflectance is somewhat in error. Considering all sources of error that are apparent to us, we estimate the maximum error to be about 5%. Even that is not sufficient to get agreement. It seems, then, that the shape of the reflectance curve is determined mainly by the free-electron character of Zn, but that it is shifted down in magnitude by the effect of core states and interband transitions.

[16] N. F. Mott and H. Jones, *The Theory of the Properties of Metals and Alloys* (Dover Publications, Inc., New York, 1958).

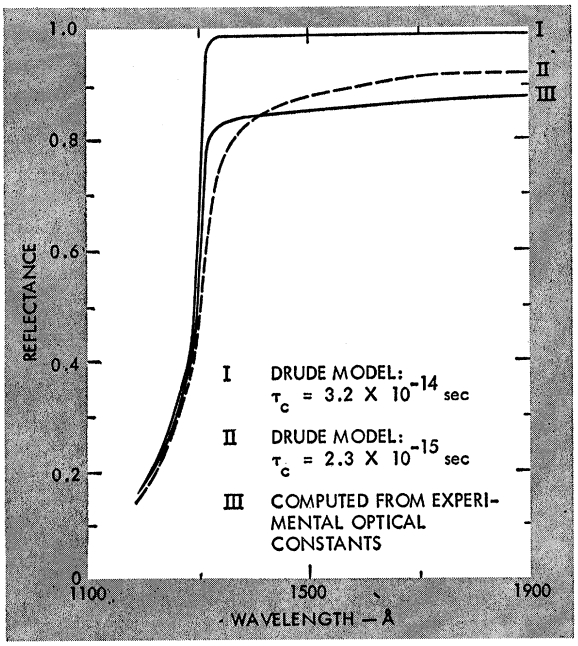

FIG. 7. Reflectance at normal incidence for basal plane of Zn.

PLASMA RESONANCE AND INTERBAND TRANSITIONS

We have associated ω_{p_a} with the sharp drop in reflectance at 1310 Å. This drop in reflectance is characteristic of a free-electron gas at the plasma frequency.[16] The true plasma frequency, however, is determined by the condition that $\epsilon_2(\omega)\ll1$ when $\epsilon_1(\omega)=0$. This condition is not well satisfied for Zn. Nonetheless, the energy-loss function (Fig. 6) has a distinct maximum, and it is this maximum that defines the true plasma frequency, ω_p. That ω_p is greater than ω_{p_a} follows directly from the influence of the low-energy interband transitions. The contribution of interband transitions to the dielectric function can be expressed as

$$\epsilon^{(b)}(\omega)=\frac{4\pi e^2}{m}\sum_j\frac{nf_j}{\omega_j^2-\omega^2-i\omega\tau^{-1}}. \tag{10}$$

For the case of interband transitions in a narrow energy range such that $\omega^2\gg\omega_j^2\gg\tau^{-2}$, a condition that holds fairly well for Zn when ω is well into the vacuum ultraviolet, Eq. (10) yields

$$\epsilon_1^{(b)}(\omega)=-(4\pi e^2N_a/m\omega^2)n_b, \tag{11}$$

$$\epsilon_2^{(b)}(\omega)=-(4\pi e^2N_a/m\omega^3\tau)n_b, \tag{12}$$

where n_b is the effective number of electrons participating in interband transitions. From Eq. (11) we see that these transitions make a negative contribution to

$\epsilon_1(\omega)$ and so shift to higher frequencies the point at which $\epsilon_1(\omega)=0$.

In our discussion so far, we have assumed that interband transitions are restricted to the visible and infrared regions. It may be that in the region of the plasma frequency, or just above it, transitions from $3d$ states begin to play a role. Calculations indicate that the d states lie just below the bottom of the valence band, that is, about 11 eV below the Fermi energy.[17] This agrees also with the value of 10.6 eV for the $M_{4,5}$ levels calculated from soft x-ray data.[18] These energies lie in a difficult region for experimental work. Thus, in the absence of more definite data, the scatter shown in $\epsilon_1(\omega)$ and $\epsilon_2(\omega)$ above the plasma frequency (Fig. 5) must be attributed largely to experimental errors, not to d states.

The value for the true plasma frequency found here ($\hbar\omega_p=10.1$ eV) is close to that ($\hbar\omega_p=9.8$ eV) found by Arakawa *et al.*[19] from experiments on optical emission of electron-bombarded thin films and characteristic energy loss. Robins[20] found $\hbar\omega_p=8.6$ eV in a characteristic energy-loss experiment, but it has been suggested that the value 8.6 eV was obtained because of an inability to resolve the volume plasmon from the surface plasmon loss at 7.1 eV.[19] It should be noted that the latter interpretation represents a change from earlier suggestions that $\hbar\omega_p=8.6$ eV corresponds to a surface plasmon.[21]

SUM RULES

It is of interest to see how the sum rules

$$\int_0^\infty \omega\epsilon_2(\omega)d\omega=\tfrac{1}{2}\pi\omega_p^2, \tag{13}$$

$$-\int_0^\infty \omega\,\mathrm{Im}\left(\frac{1}{\epsilon}\right)d\omega=\tfrac{1}{2}\pi\omega_p^2, \tag{14}$$

are satisfied for Zn. Following the procedure of Ehrenreich *et al.*,[15] we define these integrals for a finite range in terms of the effective number of electrons per atom contributing to the optical properties over that range. Thus, for example,

$$\int_0^{\omega_0} \omega\epsilon_2(\omega)d\omega=\tfrac{1}{2}\pi\left(\frac{4\pi N_a e^2}{m}\right)n_{\mathrm{eff}}(\omega_0). \tag{15}$$

Figure 8 shows the behavior of n_{eff} for Zn as obtained from a numerical evaluation of the two integrals using experimental data. The curve in Fig. 8 corresponding to Eq. (14) was evaluated using our experimental data. The curve corresponding to Eq. (13) was evaluated as follows: At long wavelengths, before the onset of interband transitions, only free-electron effects need be considered. Then, using Eq. (5), we obtain

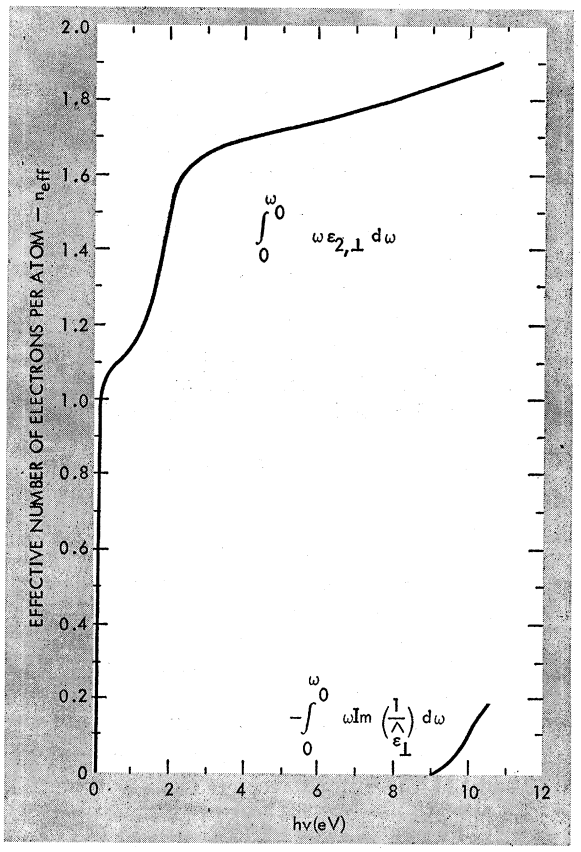

FIG. 8. Effective number of electrons per atom versus energy. The upper curve corresponds to a sum rule related to the rate of energy absorption from transverse fields (photons). The lower curve corresponds to the rate of energy absorption for longitudinal fields (electrons).

$$\int_0^{\omega_0} \omega\epsilon_2(\omega)d\omega=\omega_{p_a}^2\tan^{-1}(\omega_0\tau_c). \tag{16}$$

We have previously shown τ_c to be about 3.2×10^{-14} sec as determined from electrical conductivity for temperatures near 96°K. Thus $\omega_0\tau_c\gg1$ in the wavelength region just before the onset of interband transitions, and Eq. (16) becomes

$$\int_0^{\text{infrared}} \omega\epsilon_2 d\omega=\tfrac{1}{2}\pi\omega_{p_a}^2. \tag{17}$$

We have already seen that this corresponds to $n_{\mathrm{eff}}=0.98$.

In the near-infrared and visible ranges, corresponding to the region of strong interband transitions, we have used the data of Lenham *et al.*[1–3] and Lettington.[4] In the vacuum ultraviolet we have used our own data.

[17] R. W. Stark and L. M. Falicov, Phys. Rev. Letters **19**, 795 (1967).
[18] A. E. Sandstrom, in *Handbuch der Physik*, edited by S. Flügge (Springer-Verlag, Berlin, 1957), Vol. 30, p. 226.
[19] E. T. Arakawa, R. N. Hamm, W. F. Hanson, and T. M. Jelinek, in *Optical Properties and Electronic Structure of Metals and Alloys*, edited by F. Abeles (North-Holland Publishing Co., Amsterdam, 1966).
[20] J. L. Robins, Proc. Phys. Soc. (London) **A78**, 1177 (1961).
[21] R. J. Herickhoff, E. T. Arakawa, and R. D. Birkhoff, Phys. Rev. **137**, A1433 (1965).

The n_{eff} plot corresponding to Eq. (13) approaches the value 2, the number of valence electrons in Zn, but it is not an asymptotic approach as, e.g., in the case of Al.[15] The n_{eff} plot corresponding to Eq. (14) beings to increase only near the plasma frequency. The absence of saturation in these cases is perhaps related to the presence of d states within a few eV of the valence band. Even so, the curve corresponding to Eq. (13) is quite simple.

Note added in proof. The reflectance was measured at 100 Å intervals for $\lambda > 1600$ Å, and at 25 Å intervals at shorter wavelengths. The curves in Fig. 3 are drawn exactly through the measured reflectances. The rms deviation between the calculated optical constants and the smooth curves shown in Figs. 4 and 5 is about 5% for $\lambda > 1400$ Å; it is about 10% for $\lambda < 1400$ Å.

ACKNOWLEDGMENTS

We wish to thank T. Huen for helpful discussions and advice concerning many aspects of the experimental work, J. A. Pastrone for many valuable suggestions in the design of the sample chamber and reflectometer system and for its actual construction, and P. H. Jacob and B. Sellick for help with the experiments.

PHYSICAL REVIEW VOLUME 171, NUMBER 3 15 JULY 1968

Magnetoresistance of Potassium

JOHN R. REITZ AND A. W. OVERHAUSER
Scientific Laboratory, Ford Motor Company, Dearborn, Michigan
(Received 3 November 1967)

The linear magnetoresistance of single-crystal specimens of potassium, which is observed far into the high-magnetic-field regime, is not in accord with generally accepted ideas concerning the bands structure of potassium. The linear dependence of resistivity on field is, however, in accord with a charge-density-wave model for the metal. The charge-density wave modifies the Fermi surface by introducing many energy gaps that slice the Fermi surface. These heterodyne gaps undergo progressive magnetic breakdown. The model predicts the largest magnetoresistance for crystals in which the magnetic field is oriented along the [100] or [111] directions, and the smallest effect for crystals in which **H** is oriented parallel to [110]; these predictions are in agreement with observation.

I. INTRODUCTION

ONE of the most puzzling and unexplained observations on the alkali metals is that of their magnetoresistance: first, that they show mangetoresistance at all, and secondly, that the magnetoresistivity is linear in field to the highest magnetic fields measured.[1,2] Attempts to explain away the magnetoresistance as due to probe effects have not succeeded since probeless techniques also yield a linear change in resistance with field.[3] Recently, Penz and Bowers[4] used the helicon method to determine the magnetoresistivity of single-crystal specimens of high-purity potassium to fields of 55 kG and of polycrystalline potassium to 110 kG. Although the results show the magnetoresistivity to vary somewhat with crystallographic direction, it again is linear in field over the range studied.

It is well known that a degenerate electron gas with a spherical Fermi surface shows no magnetoresistance, and with a closed (although not necessarily spherical) Fermi surface shows constant magnetoresistance in large magnetic fields. It is generally believed that the alkali metals can be characterized by such a model and that their Fermi surfaces (at least those of sodium and potassium) deviate only very slightly from sphericity.[5] Even if the Fermi surfaces are more complicated than is generally believed, it is difficult to understand the *linear* magnetoresistance; theory predicts[6] that the transverse magnetoresistance should saturate in the high-field regime if all orbits are closed, but should vary as H^2 for certain crystallographic directions if open orbits are present. (The situation is somewhat different in compensated metals, but here again the only predicted behavior at high fields is an H^2 dependence or saturation.) Once open orbits are admitted, an approximately linear magnetoresistance over a restricted range of magnetic fields might be obtained through an averaging over various pieces of the Fermi surface. But to achieve this result, a complicated Fermi surface would be required. Since the Fermi surfaces of the alkali metals are generally thought to be simple (and closed) the resistance versus field ought to saturate for $\omega_c\tau > 1$, whereas experimentally it remains linear to $\omega_c\tau \approx 100$. (Here ω_c is the cyclotron frequency and τ is the relaxation time for scattering of electrons.)

[1] E. Justi, Ann. Physik **3**, 183 (1948).
[2] D. K. C. MacDonald, in *Handbuch der Physik*, edited by S. Flügge (Springer-Verlag, Berlin, 1956), Vol. 14, p. 137.
[3] F. E. Rose, Ph.D. thesis, Cornell University, 1964 (unpublished).
[4] P. A. Penz and R. Bowers, Solid State Commun. **5**, 341 (1967); P. A. Penz, Ph.D. thesis, Cornell University, 1967 (unpublished).
[5] D. Shoenberg and P. J. Stiles, Proc. Roy. Soc. (London) **A281**, 62 (1964); M. J. G. Lee, *ibid.* **A295**, 440 (1966).
[6] I. M. Lifshitz, M. Ya. Azbel, and M. I. Kaganov, Zh. Eksperim. i Teor. Fiz. **31**, 63 (1956) [English transl.: Soviet Phys.—JETP **4**, 41 (1957)].

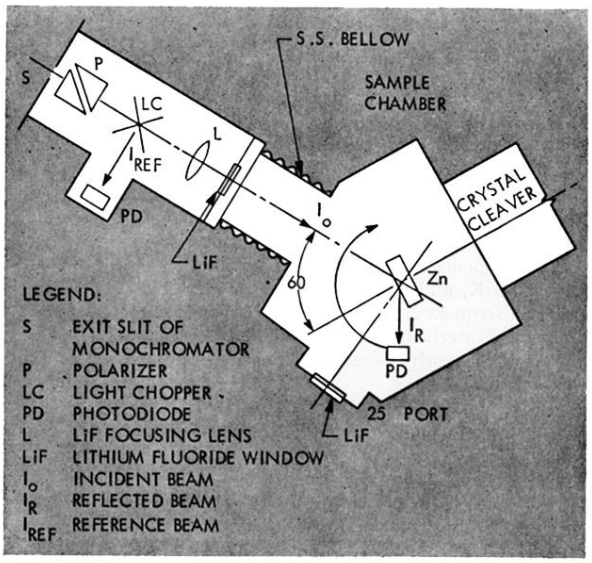

FIG. 1. Schematic drawing of vacuum reflectometor.

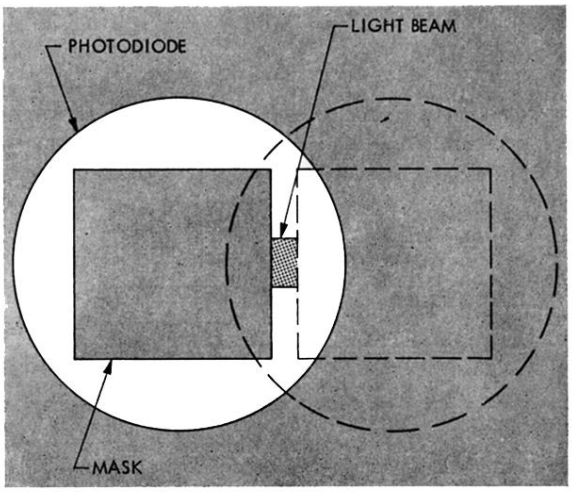

FIG. 2. Illustration of angle-of-incidence measurement.

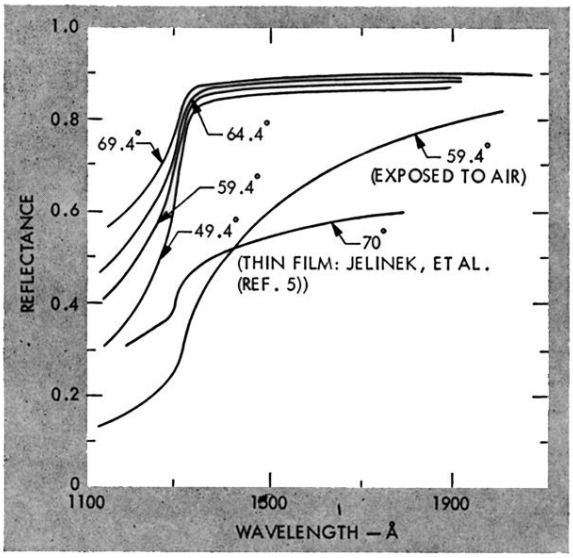

FIG. 3. Reflectance of Zn for nonpolarized light.

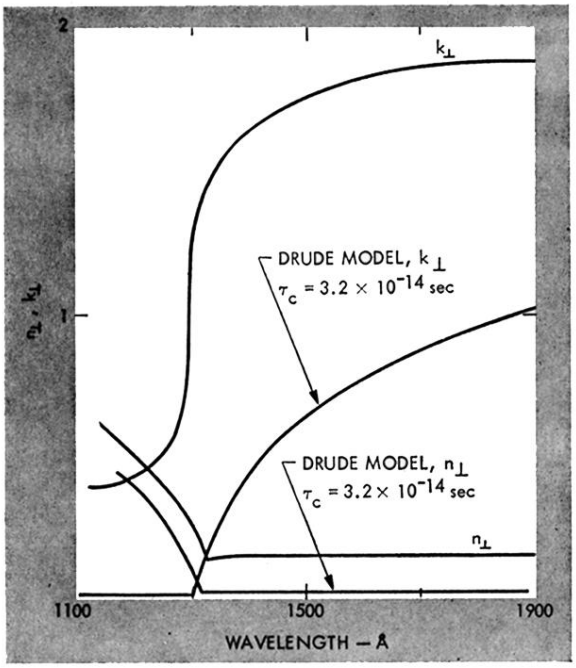

FIG. 4. Optical constants for basal plane of Zn.

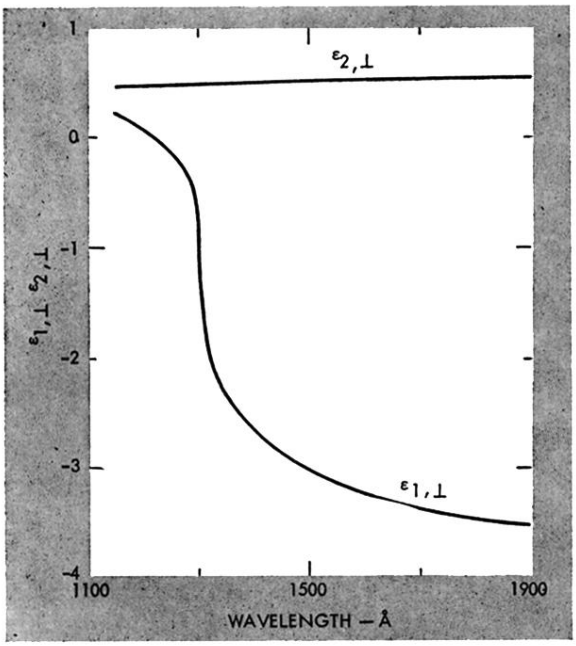

FIG. 5. Dielectric functions for basal plane of Zn.

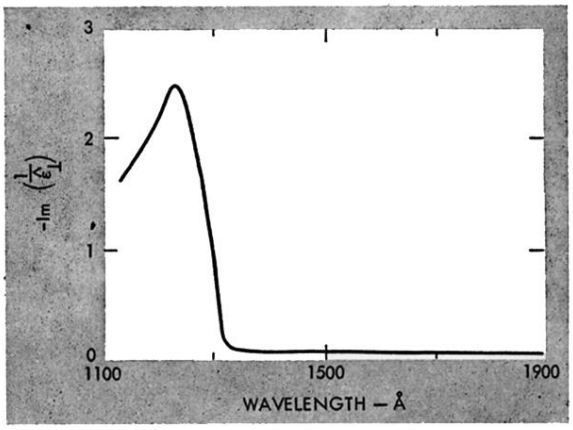

FIG. 6. Energy-loss function for basal plane of Zn.

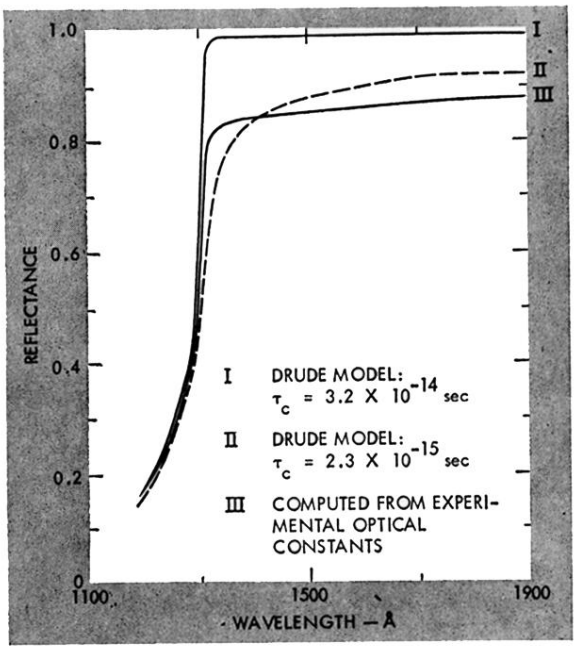

FIG. 7. Reflectance at normal incidence for basal plane of Zn.

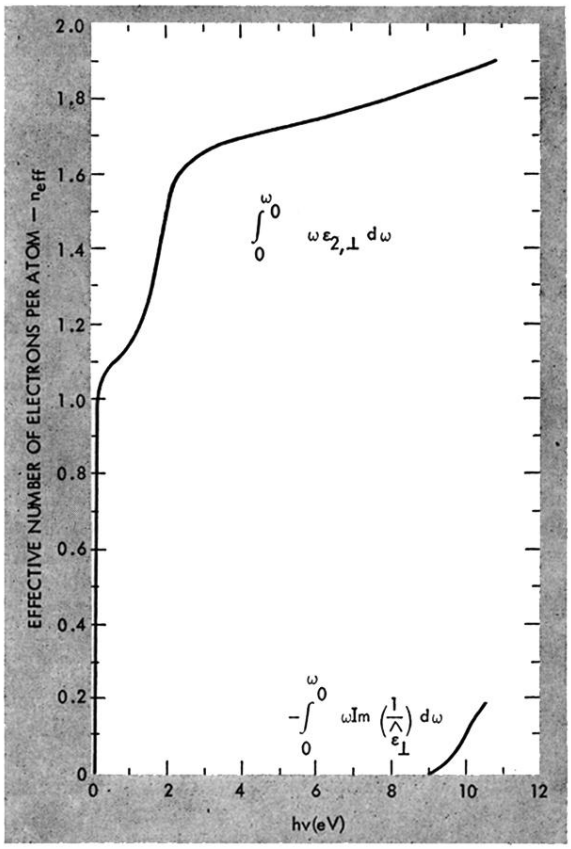

FIG. 8. Effective number of electrons per atom versus energy. The upper curve corresponds to a sum rule related to the rate of energy absorption from transverse fields (photons). The lower curve corresponds to the rate of energy absorption for longitudinal fields (electrons).